Article

Long-Range Influence of Carbohydrates on the Solvation Dynamics of Water#Answers from Terahertz Absorption Measurements and Molecular Modeling Simulations

M. Heyden, E. Bründermann, U. Heugen, G. Niehues, D. M. Leitner, and M. Havenith

J. Am. Chem. Soc., **2008**, 130 (17), 5773-5779 • DOI: 10.1021/ja0781083 • Publication Date (Web): 05 April 2008

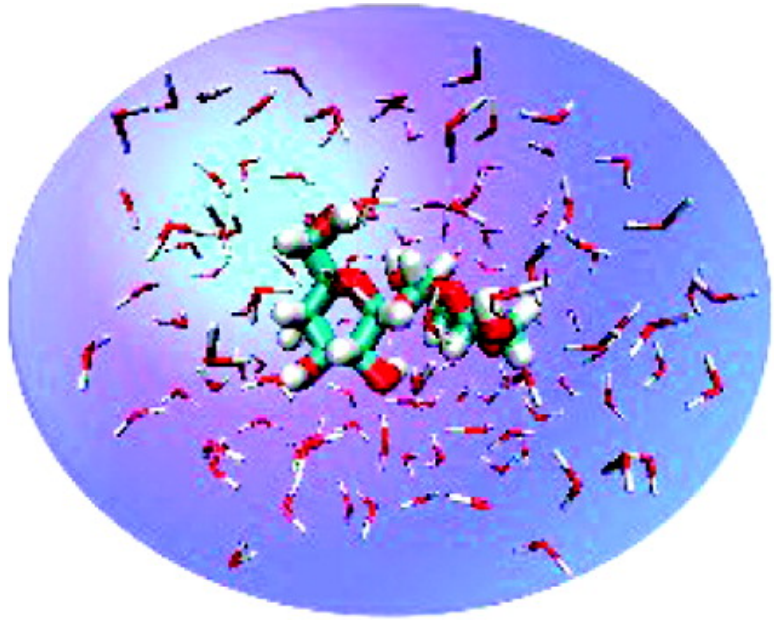

J|A|C|S
ARTICLES

Published on Web 04/05/2008

Long-Range Influence of Carbohydrates on the Solvation Dynamics of Water—Answers from Terahertz Absorption Measurements and Molecular Modeling Simulations

M. Heyden,[†] E. Bründermann,[†] U. Heugen,[†] G. Niehues,[†] D. M. Leitner,[‡] and M. Havenith*,[†]

Lehrstuhl für Physikalische Chemie II, Ruhr-Universität Bochum, 44780 Bochum, Germany, and Department of Chemistry, University of Nevada, Reno, Nevada 89557

Received October 25, 2007; E-mail: martina.havenith@rub.de

Abstract: We present new terahertz (THz) spectroscopic measurements of solvated sugars and compare the effect of two disaccharides (trehalose and lactose) and one monosaccharide (glucose) with respect to the solute-induced changes in the sub-picosecond network dynamics of the hydration water. We found that the solute affects the fast collective network motions of the solvent, even beyond the first solvation layer. For all three carbohydrates, we find an increase of 2−4% in the THz absorption coefficient of the hydration water in comparison to bulk water. Concentration-dependent changes in the THz absorption between 2.1 and 2.8 THz of the solute−water mixture were measured with a precision better than 1% and were used to deduce a dynamical hydration shell, which extends from the surface up to 5.7 ± 0.4 and 6.5 ± 0.9 Å for the disaccharides lactose and trehalose, respectively, and 3.7 ± 0.9 Å for the glucose. This exceeds the values for the static hydration shell as determined, for example, by scattering, where the long-range structure was found to be not significantly affected by the solute beyond the first hydration shell. When comparing all three carbohydrates, we found that the solute-induced change in the THz absorption depends on the product of molar concentration of the solute and the number of hydrogen bonds between the carbohydrate and water molecules. We can conclude that the long-range influence on the sub-picosecond collective water network motions of the hydration water is directly correlated with the average number of hydrogen bonds between the molecule and adjacent water molecules for carbohydrates. This implies that monosaccharides have a smaller influence on the surrounding water molecules than disaccharides. This could explain the bioprotection mechanism of sugar−water mixtures, which has been found to be more effective for disaccharides than for monosaccharides.

Introduction

It has been long known that some micro-organisms and plants can withstand dehydration and extreme-cold conditions for extended periods. The ability to survive such extreme conditions, or anhydrobiosis, is apparently correlated with the presence of increased amounts of soluble disaccharides, in particular trehalose. Although this bioprotection mechanism is widely used in industrial processes, its molecular mechanism is still a source of controversy. The first report on the role of trehalose as a stabilizer for cells and membranes leading to anhydrobiosis was presented by Crowe and co-workers.[1] They found that in the presence of trehalose, dry dipalmitoyl phosphatidylcholine (DPPC) freezes at a temperature that is 30 °C lower than the freezing point of DPPC without trehalose. Interaction of trehalose with DPPC was suspected to be responsible for the ability of trehalose to stabilize dry membranes in anhydrobiotic organisms. The underlying mechanism was thought to result from hydrogen bonding of the OH groups in the carbohydrates with the polar head groups of DPPC. The relative effectiveness in preserving the structural and functional integrity of membranes for the different carbohydrates was found to decrease from trehalose, lactose, and maltose to glucose and glycerol.[2] The most recent study on the role of trehalose as a stabilizer demonstrated the use of trehalose to stabilize human blood platelet mammalian cells.[3] Since then, numerous studies have been carried out with the aim of investigating the underlying molecular mechanism of the bioprotection of sugars.

The concept of biological water, that is, the water surrounding biological molecules is dynamically distinct from bulk water,[4] has led to the speculation that the solute-induced changes of the hydration dynamics within the hydration shell result in retardation of the water dynamics near biological molecules. For trehalose in particular, it has been further speculated that the strong bioprotection effect may result from this retardation of the surrounding water, possibly via the coupling of the trehalose motions to the hydration water.[5,6] Because protein and

[†] Ruhr-Universität Bochum.
[‡] University of Nevada.

(1) (a) Crowe, J. H.; Crowe, L. M.; Chapmann, D. *Science* **1984**, *223*, 701. (b) Crowe, J. H.; Crowe, L. M. *Nat. Biotechnol.* **2000**, *18*, 145.
(2) Crowe, L. M.; Mouradian, R.; Crowe, J. H.; Jackson, S. A.; Womersly, C. *Biochim. Biophys. Acta* **1984**, *769*, 141–150.
(3) Crowe, J. H.; Crowe, L. M.; Wolkers, W. F.; Oliver, A. E.; Ma, X.; Auh, J. H.; Tang, M.; Zhu, S.; Norris, J.; Tablin, F. *Integr. Comp. Biol.* **2005**, *45*, 810–820.
(4) Pal, S. K.; Peon, J.; Bagchi, B.; Zewail, A. H. *J. Phys. Chem. B* **2002**, *106*, 12376–12395.

water dynamics are indeed coupled, any retardation in the surrounding water network dynamics as induced by the addition of trehalose to the surrounding buffer might therefore directly influence the protein dynamics.

A recent study showed that protein folding has the same temperature dependence as the α-fluctuations, which is the relaxation dynamics, which are probed by dielectric spectroscopy.[7] The large-scale protein motions are shown to follow the solvent fluctuations; however, because of the large number of steps involved, the former one is slower by orders of magnitude. For example, the temperature-dependent rate coefficient for the exit of CO or O_2 from myoglobin $k_{exit}(T)$ parallels $k_\alpha(T)$ over almost 6 orders of magnitude but is slower by nearly 5 orders of magnitude.[7] Molecular dynamics (MD) simulations reveal the existence of rather rigid water structures around proteins[8] and carbohydrates.[9] The retardation of water hydrogen-bond dynamics found in the MD studies is detected experimentally by depolarized Rayleigh scattering.[10] Kilburn et al. have recently discussed a pure structural concept explaining the changes in the organization and mobility of water in amorphous and crystalline trehalose.[11] By using positron annihilation lifetime spectroscopy, they found that in the crystalline dehydrate, water is confined to one-dimensional well-organized channels, which might serve as sink and source in low-moisture systems. They postulate this static description as a possible molecular explanation for the efficiency of trehalose in bioprotection.

In recent studies, we demonstrated that terahertz (THz) spectroscopy is able to probe directly the change of the fast water network motions within a certain distance around solutes, which we call the dynamical hydration layer.[12,13] By a precise measurement of absorption coefficients between 2.3 and 2.9 THz, we could estimate the size and the characteristics of this dynamical hydration shell. Our previous study for lactose showed a non-linear concentration dependence of the total THz absorption at low concentrations (0−2 mol/L). This indicated that solvation water molecules within this dynamical hydration shell exhibit enhanced absorption. The dynamical hydration shell extends to 5.13 ± 0.24 Å from the surface of the disaccharide, which corresponds to about 2 solvation layers.[12] The appearance of the nonlinearity in the concentration dependence of the absorption coefficient is attributed to the solute-induced change in the THz absorption of the hydration water. We found an absorption coefficient for this hydration water that is distinct from that of bulk water. Accompanying MD simulations on lactose were consistent with these results and indicated a retardation of the typical hydrogen-bond dynamics. The hydrogen-bond lifetime for bonds between water molecules in the bulk was computed to be 1.25 ps, compared with 1.9 ps for water molecules in the first solvation layer. The results indicated significant retardation of hydrogen-bond dynamics up to 6 Å from the lactose surface, which exceeds the first solvation shell of ca. 3 Å.

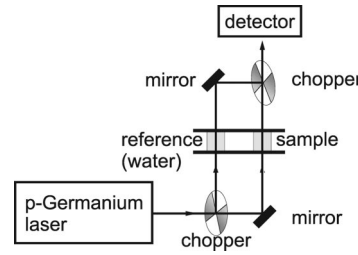

Figure 1. Experimental setup. Displayed is the path of the THz radiation. The mirror chopper splits the radiation into two distinct beams. The radiation passes alternately through the bulk water and through the sugar solution. The transmitted radiation is then focused onto the detector.

Here, we extend our initial study on lactose and provide a direct systematic comparison between the THz spectra and the dynamics of solvated mono- and disaccharides. Moreover, we present here the result of more-detailed simulation studies. We will show that the solute-induced change in hydration dynamics is directly related to the number of hydrogen bonds formed between water molecules and the sugar. Accompanying molecular modeling calculations support most trends observed experimentally and provide a microscopic visualization of the underlying molecular mechanism.

Experimental Section

We have used our THz spectrometer in Bochum to investigate the dynamics of the hydration shell around carbohydrates. The setup uses a table-top p-Ge laser as a high-power (2 W) THz radiation source, which allows us to penetrate water to a thickness of 150 μm.[14] We were able to study solvated sugars from the dilute to the high concentration limit. The frequency range of the spectrometer (1−4 THz) accesses the intermolecular collective modes of the hydrogen-bonding network and low-frequency modes of the saccharides. As has been demonstrated by us before, the relevant information for the study of the coupled solute−water dynamics is provided not by a measurement of frequency-dependent THz absorption but by a precise measurement of the solute-induced changes in the THz absorption coefficient as a function of the solute concentration.[12] Additional frequency-dependent intensity measurements show a linear increase of the absorption between 1 and 3 THz and do not yield any additional information. We have therefore restricted the measurements to the range from 2.1 to 2.9 THz, where the difference between bulk water and hydration water is larger than that for lower frequencies, but the output power of the laser is still high.

The accuracy of the determination of the absorbance and size of the dynamical hydration shell depends directly on the precision of the measured concentration-dependent changes in the THz absorption coefficient, $\alpha(c)$, where c is the concentration, at a particular temperature. Compared to previous measurements,[12] we have considerably improved the accuracy of $\Delta\alpha$, the difference between the concentration-dependent absorption coefficient of the saccharide solution and that of bulk water. The new experimental setup is shown in Figure 1.

The transmitted intensities were measured at a fixed layer thickness by using a standard Bruker liquid sample cell with Teflon

(5) Massari, A. M.; Finkelstein, I. J.; McClain, B. L.; Goj, A.; Wen, X.; Bren, K. L.; Loring, R. F.; Fayer, M. D. *J. Am. Chem. Soc.* **2005**, *127*, 14279–14289.
(6) Magazù, S.; Villari, V.; Migliardo, P.; Malsano, G.; Telling, M. T. F. *J. Phys. Chem. B* **2001**, *105*, 1851–1855.
(7) Frauenfelder, H.; Fenimore, P. W.; Chen, G.; McMahon, B. A. *Proc. Natl. Acad. Sci. U.S.A.* **2006**, *103*, 15469–15472.
(8) Bizzarri, A. R.; Cannistraro, S. *J. Phys. Chem. B* **2002**, *106*, 6617–6633.
(9) Lee, S. L.; Debenedetti, P. G.; Errington, J. R. *J. Chem. Phys.* **2005**, *122*, 204511–204519.
(10) Paolantoni, M.; Sassi, P.; Morresi, A.; Santini, S. *J. Chem. Phys.* **2007**, *127*, 024504.
(11) Kilburn, D.; Townrow, S.; Meunier, V.; Richardson, R.; Alam, A.; Ubbink, J. *Nat. Mater.* **2006**, *5*, 632–635.
(12) Heugen, U.; Schwaab, G.; Bründermann, E.; Heyden, M.; Yu, X.; Leitner, D. M.; Havenith, M. *Proc. Natl. Acad. Sci. U.S.A.* **2006**, *103*, 12301.
(13) Ebbinghaus, S.; Kim, S. J.; Heyden, M.; Yu, X.; Gruebele, M.; Leitner, D. M.; Havenith, M. *Proc. Natl. Acad. Sci. U.S.A.* **2007**, *104*, 20749.
(14) Bergner, A.; Heugen, U.; Bründermann, E.; Schwaab, G.; Havenith, M.; Chamberlin, D. R.; Haller, E. E. *Rev. Sci. Instrum.* **2005**, *76*, 63110–63115.

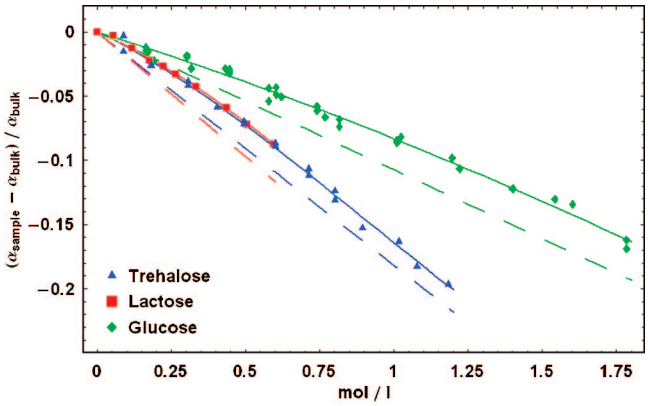

Figure 2. Difference in the integrated THz absorption coefficient (2.1−2.8 THZ) relative to bulk water plotted against the concentration of trehalose (blue), lactose (red), and glucose (green). The temperature is kept at 20 °C. The statistical experimental uncertainty for each measurement is smaller than the size of the dot ($\Delta((\alpha_{sample} - \alpha_{bulk})/\alpha_{bulk}) = \pm 0.008$). For comparison, the dashed lines show the predicted concentration dependence of the THz absorption of a two-component model when we consider only the replacement of water molecules by the increasing number of carbohydrates. In this case, we expect a linear decrease of the overall THz absorption with increasing concentration of the solute. The measured THz absorbance reveals a nonlinear concentration dependence, indicating overlapping hydration shells.

spacers and z-cut quartz windows. The layer thickness of the aqueous sample, which is placed between two parallel quartz windows, was determined to be 52.6 ± 0.3 μm by using FTIR spectroscopy to record the etalon fringes.

As a THz radiation source, we used our p-Ge laser, which has been described in detail in ref 14. This radiation source has a high output power of ca. 1 W. The repetition rate is 70 Hz which is restricted by the speed of the chopper and the synchronizing electronics. The THz pulse trains were split into two radiation pathways by using a mirror chopper. The sample was placed in one of them, and every second pulse was directed to the second path which contained bulk water as a reference. The temperature of both samples was kept constant at 20 °C ± 0.1 °C. The detector consisted of an Al-doped Ge crystal, cooled down to 4 K, which acts as a sensitive photoconductor above 1.6 THz. The incoming THz radiation causes a voltage drop at the detector, which is amplified and recorded in an oscilloscope.

For each concentration c, 5000 pulses were sampled, and the average pulse intensities I were fitted to the following expression: $I = I_0 \exp(-\alpha\, d) + C$, with I_0, α, d, and C corresponding to the intensity before the probe, the absorption coefficient of the probe, the layer thickness of the probe, and the detector offset, respectively. We have measured the THz spectra of the different sugars with increasing concentration up to the highest concentration which was still soluble (0.6 mol/L for lactose, 1.2 mol/L for trehalose, and 1.8 mol/L for glucose; see Figure 2).

For a determination of the dynamical hydration shell, a precise (uncertainty of less than 1%) measurement of the changes in the total absorption coefficient with concentration is required. The previous measurements on lactose showed a linear increase of the absorption of the carbohydrate solutions with frequency in the frequency range from 2.4 to 3.0 THz.[12] Therefore, for each solute concentration, the frequency-resolved measurements were each fitted to a linear function, and the result was used for further analysis. In the new setup, we abandoned a frequency selection by a grating, and instead, the integrated THz absorption between 2.1 and 2.8 THz, which yields a better signal-to-noise ratio, was recorded. In Figure 2, the integrated THz absorption coefficient compared to buffer ($\alpha_{rel} = (\alpha(c) - \alpha(0))/\alpha(0)$) is plotted against the carbohydrate concentration, c ($\alpha(0) = 420\ cm^{-1}$).

One might naively expect a linear decrease of the THz absorption coefficient because the solute molecules replacing the water have far fewer low-frequency modes than the solvent they replace. This leaves a hole in the spectral density of the low-frequency modes of the solute−water mixture because sugar molecules can be considered as almost-transparent balls in the THz range.[15] However, for all carbohydrates, we find a characteristic onset of nonlinearity at a specific concentration c_0, which is directly related to the size of the dynamical (THz) hydration shell. In Figure 2, we summarize the results of our new measurements for glucose, lactose, and trehalose.

When comparing these data to the results of our previous study on lactose,[12] we find that the experimental uncertainty of each single measurement has decreased considerably. This can be attributed to the fact that instead of subsequently measuring the solvent and bulk water, we have directly probed the difference between solvated sugars and the bulk water. Both samples were measured simultaneously, which implies that any systematic errors due to small drifts in temperature and humidity are eliminated.

Fit of the Experimental Data. We have also fitted the experimental data of the concentration-dependent THz absorption coefficients to an empirical three-component model which was introduced in our previous paper.[12] The total absorbance is attributed to the absorption of the carbohydrate α_{solute}, the water in the hydration shell α_{shell}, and the bulk water α_{bulk}. Accordingly, we distinguish between three volume fractions representing the partial volume of the carbohydrate molecules V_{solute}, the volume in the hydration shell around the carbohydrates V_{shell}, and the remaining partial volume of the bulk water $V_{bulk} = V_{total} - V_{solute} - V_{shell}$.

According to the model, the overall absorption of the system can be described by:

$$\alpha_{total}(\omega) = \frac{V_{solute}(c)}{V_{total}}\alpha_{solute}(\omega) + \frac{V_{shell}(c, \delta R)}{V_{total}}\alpha_{shell}(\omega) + \left(1 - \frac{V_{shell}(c, \delta R)}{V_{total}} - \frac{V_{solute}(c)}{V_{total}}\right)\alpha_{bulk}(\omega) \quad (1)$$

Here α_{total}, α_{solute}, α_{shell}, and α_{bulk} are the absorption coefficient of the solution, the absorption coefficient of the solute, the absorption coefficient of the solvation water, and the absorption coefficient of the bulk water, respectively. V_{total}, V_{solute}, and V_{shell} are the total volume, the volume of the solute molecules, and the volume occupied by the dynamical hydration shell, that is, the part of the water around the solute that is affected by the solute, respectively. The water in the dynamical hydration shell has a THz absorption coefficient which is distinct from that of bulk water. The model assumes a step transition to bulk water at a certain distance δR from the sugar surface. The assumption of a stepwise transition from hydration water to bulk water is certainly only a first approximation. However, we know from our previous studies that more sophisticated models, such as models with a nonspherical assumption, lead to the same results within the experimental uncertainty.[12]

If the hydration layers overlap, the absorption coefficient of the hydration water is assumed to be unaffected. This is confirmed by our molecular modeling calculations and further supported by the study of Mason.[16] The dynamical hydration shell is defined as the layers of water in which the global network oscillations as probed by THz spectroscopy are affected by the carbohydrate. This is distinct from a static hydration shell; a study by Magazù et al. yielded hydration numbers (number of water molecules in the hydration layer) between 7.5 and 9, in agreement with hydration numbers for disaccharides as evaluated from previous ultrasonic measurements (14−15).[6] A more recent neutron-diffraction study by Mason et al. concluded that the long-range structure of water is

(15) Jockusch, R. A.; Kroemer, R. T.; Talbot, F. O.; Snoek, L. C.; Çarçabal, P.; Simons, J. P.; Havenith, M.; Bakker, J. M.; Compagnon, I.; Meijer, G.; von Helden, G. *J. Am. Chem. Soc.* **2004**, *126*, 5709–5714.
(16) Mason, P. E.; Neilson, G. W.; Enderby, J. E.; Saboungi, M. L.; Brady, J. W. *J. Phys. Chem. B* **2005**, *109*, 13104–13111.

Table 1. Result of the Fit of the Dynamical Hydration Shell[a]

	α_{solute} (cm^{-1})	$V_{solute}/V_{m,water}$[b]	α_{shell} (cm^{-1})[c]	$V_{shell}/V_{m,water}$[b]	δR (Å)
glucose	20[19]	6.27	437.1 ± 1.8	47.3 ± 9.1	3.71 ± 0.9
lactose	30[12,18]	11.57	434.7 ± 0.9	147.6 ± 16.9	5.69 ± 0.4
trehalose	53	11.57	429.4 ± 0.7	186.4 ± 47.7	6.46 ± 0.9

[a] We fixed the absorption coefficient of the solute and the volume. Shown are the fitted absorption coefficients of the dynamical hydration shell relative to the molecular volume of one water molecule and the extension of the dynamical hydration shell from the surface of the carbohydrate. These are the results of the fit to the experimentally observed changes in THz absorption of the carbohydrate−water mixture. [b] $V_{m,water} = 18.015\ cm^3\ mol^{-1}$. [c] $\alpha_{bulk} = 420\ cm^{-1}$.

not significantly changed by the presence of the sugar solute.[16] However, the fast dynamics can be affected over a much longer range than the range which was found for static hydration shells as probed, for example, by scattering experiments. The static hydration shell was found to be restricted to the first hydration shell[15] and is determined by steric hindering and hydrogen bonding.

THz spectroscopy probes the sub-picosecond−picosecond intermolecular motions very sensitively. The THz absorption coefficient of water at 1.5 THz is changed by a factor of 4−5 between 270 and 370 K.[17] This is a larger change compared to that which is observed in other spectral regions. This makes THz spectroscopy an especially sensitive tool to probe solute-induced changes in the solvation dynamics.

The (concentration-dependent) partial volume of the carbohydrate molecules is obtained from the molecular volume, assuming that we have an ideal mixture (which was verified experimentally). The volume occupied by the dynamical hydration shell was calculated with a Monte-Carlo-like method, taking explicitly into account the effect of overlapping solvation shells: 1000 carbohydrate molecules (for simplicity, each pyranose ring was represented by one superatom) were randomly distributed and orientated in a cubic simulation box, the dimensions of which were chosen to give the targeted concentration. Overlap of two carbohydrate molecules was excluded. For a given thickness of the hydration shell, δR, the volume fraction was computed via a random-walk algorithm. δR was varied from 0.02 to 4.00 nm in steps of 0.02 nm. This was repeated 100 times to decrease the statistical error. This method was applied to concentrations ranging from 0.02 to 1.30 mol/L for trehalose and lactose and up to 2.0 mol/L for glucose, in steps of 0.02 and 0.05 mol/L.

For a final fit of the data to eq 1, $V_{shell}(c,\delta R)$ and $\alpha_{shell}(\omega)$ were varied, whereas $\alpha_{solute}(\omega)$ and $\alpha_{bulk}(\omega)$ were fixed at their experimental values.[12,18] We have used the same model and fitting routine for all three sugars to enable a direct comparison of their effects on the hydration dynamics. The results for the three carbohydrates, trehalose, lactose, and glucose, as obtained in this study are listed in Table 1.

We note that our model in eq 1 assumes THz absorption of three independent components. This would imply that the absorbing collective motion of the solute and the water would be strictly decoupled. Although molecular modeling calculations indeed reveal a coupling between the solute and solvent motions, the model fits the experimental data satisfactorily. A more sophisticated model would introduce additional parameters which cannot be related directly to the experimental data. We therefore have taken the simplest model which covers all important aspects.

Theoretical Modeling. Classical simulations were performed with the GROMACS software package. The trehalose, lactose, and glucose molecules were described by using parameters from the OPLS-all-atom force field for carbohydrates,[20] whereas the rigid SPC force field[21] was used for the water. For all simulations, a 3 × 3 × 3 nm simulation box containing different numbers of carbohydrate molecules was used with periodic boundary conditions applied in all directions. The number of carbohydrate molecules ranged from 1 to 16, corresponding to concentrations between 0.0615 and 0.984 mol/L. An initial simulation was carried out with only bulk water. In addition, a system with four molecules of trehalose and water described by the TIP3P and TIP5P force field was investigated to compare the results for the different force fields.

For each system, several statistically independent start structures with random start velocities were generated and used as starting points for extensive simulations in the NVT ensemble (i.e., constant number, volume, and temperature). Each system was simulated for 96 ns; for the trehalose solutions and bulk water, this was extended to 360 ns.

The simulations were performed by integrating the Newtonian equations of motion with a standard leapfrog algorithm by using time steps of 1 fs. The temperature was controlled by a Berendsen-type[22] thermostat and was kept constant at 300 K. Electrostatic interactions were calculated with the Particle-Mesh-Ewald method[23] by using a 0.12 nm grid and a fourth-order interpolation. The cutoff values for van der Waals and electrostatic interactions were set to 0.9 nm. The system coordinates were stored every 30 fs and used to calculate the ensemble average autocorrelation function, C_M, of the system's dipole moment, M, from 0 to 50 ps:

$$C_M(t) = \langle M(0)M(t)\rangle \tag{2}$$

For the glucose solutions, an increased time resolution of 8 fs was used.

The ensemble average dipole autocorrelation function was then used to calculate the absorption line shape function $I(\omega)$ and the absorption cross-section $\alpha(\omega)$:[24]

$$I(\omega) = \frac{1}{2\pi}\int_{-\infty}^{\infty} \mathrm{d}t\, C_M(t)\exp(i\omega t) \tag{3}$$

$$\alpha(\omega) = \frac{4\pi^2\omega(1-\exp(\hbar\omega/kT))}{3\hbar c n(\omega)} I(\omega) \tag{4}$$

The frequency dependence of the index of refraction ($n(\omega)$) in eq 4 is not taken into account here, because it is nearly constant at frequencies above 1.5 THz.[17] As a consequence, the value $n(\omega)\alpha(\omega)$ is expected to be directly proportional to the actual absorption. The result of the predicted THz absorption band for several glucose concentrations is displayed in Figure 3.

In addition, we have carried out a normal-mode analysis on the systems containing trehalose and bulk water. For every system, this was done for the local minima of the potential-energy surface found by quenching structures at 10 randomly chosen times during the simulations. The absorption strength of each normal mode was calculated to be proportional to the square of the change of the dipole moment. Each absorption line is represented by a Gaussian with a line width of 10 cm^{-1}. The average spectrum of the 10 structures was computed, and the standard deviation was used as an estimate for the error bars.

(17) Rønne, C.; Thrane, L.; Astrand, P. O.; Wallqvist, A.; Mikkelsen, K. V.; Keiding, S. R. *J. Chem. Phys.* **1997**, *107*, 5319.
(18) Fischer, B.; Jepsen, P. U.; Helm, H. Germany Patent Appl. DE 103 09 845 A1 2004.09.16, 2004.
(19) Fischer, B. M.; Franz, M.; Abbott, D. THz spectroscopy as a versatile tool for investigating crystalline structures. In Proceedings of the Joint 31st International Conference on Infrared and Millimeter Waves and 14th International Conference on Terahertz Electronics,Sept 18−22, 2006, Shanghai, China.
(20) Damm, W.; Frontera, A.; Tirado-Rives, J.; Jorgensen, W. L. *J. Comput. Chem.* **1997**, *18*, 1955–1970.
(21) Berendsen, H. J. C.; Postma, J. P. M.; van Gunsteren, W. F.; Hermans, J. In *Intermolecular Forces*; Pullman, B., Ed.; Reidel: Dordrecht, Holland, 1981; pp 331−342.
(22) Berendsen, H. J. C.; Postma, J. P. M.; van Gunsteren, W. F.; DiNola, A.; Haak, J. R. *J. Chem. Phys.* **1984**, *81*, 3684–3690.
(23) Darden, T.; York, D.; Pedersen, L. *J. Chem. Phys.* **1993**, *98*, 10089–10092.
(24) McQuarrie, D. A. *Statistical Mechanics*, University Science Books: Herndon, VA, 2000; pp 470–476..

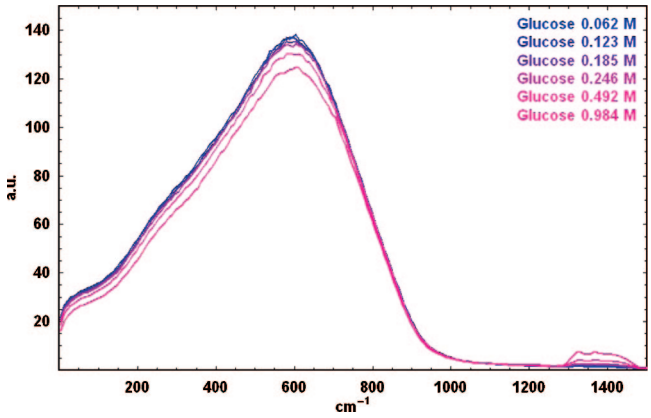

Figure 3. Simulated absorption bands of solvated glucose for distinct glucose concentrations: 0.062, 0.123, 0.185, 0.246, 0.492, and 0.984 M. The increasing glucose concentrations result in a decreasing absorption between 0 and 900 cm^{-1} and an increasing IR absorption around 1400 cm^{-1}.

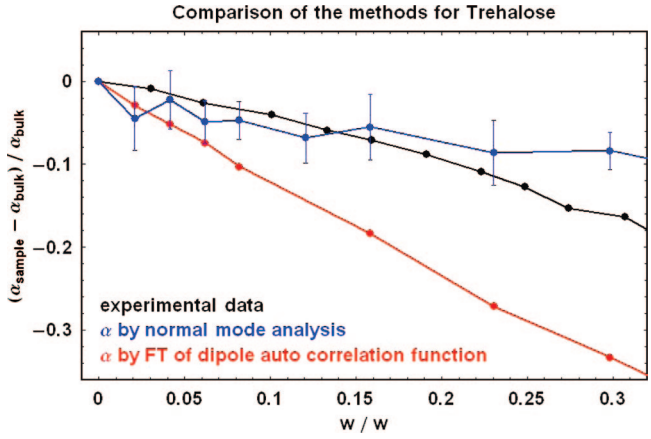

Figure 4. Simulated concentration dependence of the THz absorption coefficient (plotted against the weight fraction of trehalose) relative to bulk water at 2.55 THz (85 cm^{-1}) by using normal-mode analysis (blue) and by taking the Fourier transform of the dipole autocorrelation function (red) of the trehalose−water mixture. In black, we show the experimental results for comparison.

The results of both approaches for the calculated THz absorption coefficient of a trehalose−water mixture are shown in Figure 4, where the results are directly compared with our experimental results. The curves connect the points and just serve as a guide to the eye.

The computed absorbance exhibits a concentration dependence that is similar to the experimental one. Differences between the two computational approaches are mainly attributable to the lack of anharmonic effects in the normal-mode calculation, which are intrinsic to the dipole autocorrelation function. Still, the concentration-dependent absorbance computed with normal modes agrees better with experimental data over a broad range of concentrations than does the result obtained with the dipole autocorrelation function. Differences between the latter results and experiment are due, at least in part, to the force-field model used in the MD simulations, which is not optimal for treating water at the interface with a solute.[25] Another potential source of error in both calculations is the use of a small number of solute molecules with periodic boundary conditions, which could lead to artifacts due to alignment. However, comparison of results with one solute per box and two solutes in a box that is twice as large indicates that this effect is negligible in these simulations.

Despite the quantitative differences between the computational and experimental results, we have tried to fit the computational results to the model of eq 1. Results from the dipole autocorrelation calculation for the trehalose and glucose solutions are given in Table 2. Fitting the computational results to the three-component model yields an absorption coefficient of the hydration layer that is smaller than the absorption coefficient for bulk water, unlike the experimental results. The size of the hydration layer extracted from the computational results is similar to the one deduced from the experimental data. A previous calculation of the absorbance of lactose and hydration water by using normal modes[12] with free boundaries yielded an absorbance that was greater than the absorbance of bulk water, consistent with experiment.

Table 2. Result of the Fit of the Dynamical Hydration Shell[a]

	α_{solute} (cm^{-1})	$V_{m,solute}/V_{m,water}$[b]	α_{shell} (cm^{-1})[c]	$V_{m,shell}/V_{m,water}$[b]	δR (Å)
glucose	20[18]	6.27	368.1 ± 3.3	61.2 ± 6.2	4.3 ± 0.2
trehalose	53	11.57	320.0 ± 6.7	55.6 ± 5.9	3.2 ± 0.2

[a] We fixed the absorption coefficient of the solute and the volume. Shown are the fitted absorption coefficients of the dynamical hydration shell relative to the molecular volume of one water molecule and the extension of the dynamical hydration shell from the surface of the carbohydrate. These are the results of the fit to the simulated changes in THz absorption of the carbohydrate−water mixture. [b] $V_{m,water} = 18.015$ cm^3 mol^{-1}. [c] $\alpha_{bulk} = 420$ cm^{-1}.

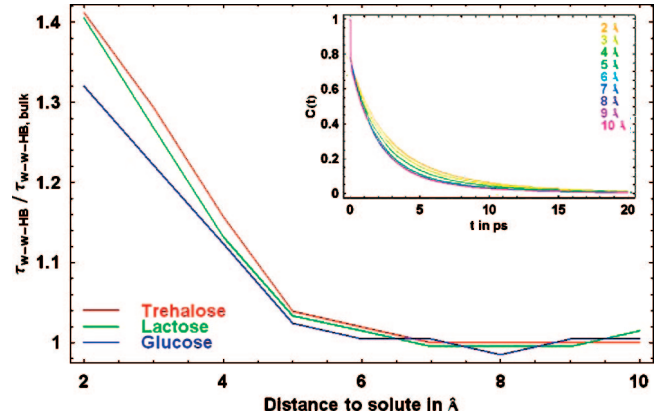

Figure 5. Average water−water hydrogen-bond lifetime relative to the bulk hydrogen-bond lifetime as a function of the distance from the solute. Displayed are results for glucose (blue), lactose (green), and trehalose (red). Inset: C-type hydrogen-bond correlation function for hydrogen bonds between water molecules in the vicinity of trehalose at different distances to the solute.

We have investigated in detail the different absorption behaviors of the water in the solvation shell. Some efforts have already been made in a recent publication by Lee et al.,[9] targeting the single-molecule rotational correlation and the self-diffusion coefficient of water molecules with different distances to the sugar molecule. In our work, the self-diffusion coefficient and the C-type hydrogen-bond lifetime, which is the time at which the survival probability of a hydrogen-bonded donor−acceptor pair decays to 1/e,[26] were analyzed for bonds between water molecules as a function of the distance from the solute by using trajectories that were calculated with the same parameters as those used for the spectrum calculation with a single trehalose molecule. For the calculation of the hydrogen-bond lifetimes, we adopted the geometric hydrogen-bond criterion by using a minimum donor–hydrogen–acceptor angle of 150° and a maximum donor−acceptor distance of 3.5 Å.

The results for the calculated C-type hydrogen-bond lifetime are shown in Figure 5. Displayed is the average water−water hydrogen-bond lifetime. A hydrogen bond can survive momentary breakage due to rotational movement of the donor or acceptor molecule, as

(25) van Maaren, P. J.; van der Spoel, D. *J. Phys. Chem. B* **2001**, *105*, 2618–2626.
(26) Bagchi, B. *Chem. Rev.* **2005**, *105*, 3197–3219.

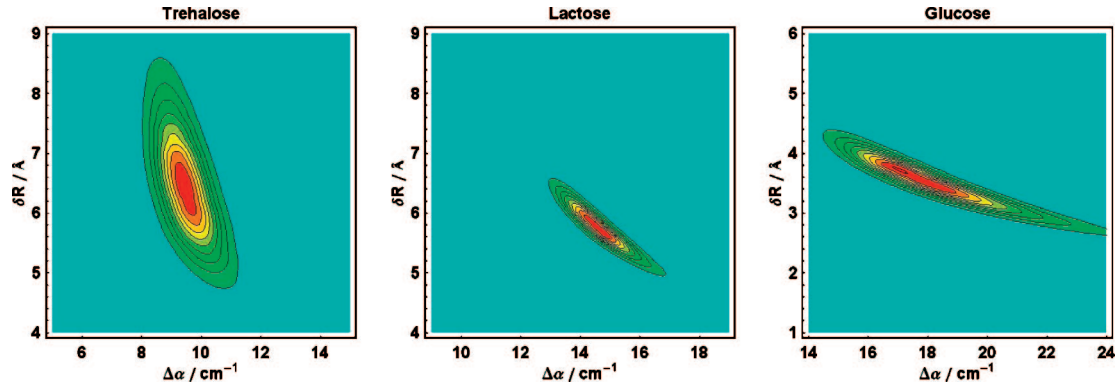

Figure 6. Contour plots of the normalized statistical likelihood of the two fitted parameters (the dynamical hydration radius and the difference in the absorption coefficient of the hydration layer and bulk water) given by the exponential of the negative sum of squares of the differences between the values of the model function and the experimental data. The contours are given in 10% steps.

long as they reconnect again later due to further rotation. This implies that the decay of the C-type hydrogen-bond correlation function is dominated by diffusional movements (and not by pure rotational motions). The lifetime significantly increases by approximately 30% (glucose) and 40% (lactose, trehalose) in the close vicinity of the carbohydrate. With increasing distance, it decreases almost linearly until it reaches the bulk water hydrogen-bond lifetime. The transition to the bulk hydrogen-bond lifetime takes place at distances between 5 and 6 Å. The inset in Figure 5 displays the C-type hydrogen-bond correlation functions for hydrogen bonds between water molecules at several distances from trehalose to visualize the slower decay of $C(t)$ at smaller distances.

Discussion

In this study, the accuracy of the measured THz absorption coefficient (typically less than ± 2 cm^{-1}) was improved substantially compared to that of our first measurements (error bars in ref 12 ± 5 cm^{-1}). With the new experimental setup, it was sufficient to include only 10−20 single measurements, compared with more than 400 previously. The small deviation of experimental data points from the best-fit curve supports the three-component model as a useful descriptor even more strongly than in our previous work, because nearly all measured points lie within one error bar of the best-fit curve. Any two-component model, taking into account only solute and bulk-water absorbance, is unable to reproduce the experimental data.

The degree and sense of the curvature of the best fit to the integrated THz absorption of the solute−water mixture depend on the relative change in the absorption coefficient of the water in the dynamical hydration shell compared to bulk water, that is, the deviation of the concentration dependence $\alpha(c)$ from the two-component model. If the solute-induced change in the absorption coefficient were negative, the initial curvature at low concentrations would be concave up (negative slope), and the curve would lie below the linear two-component prediction, rather than the concave down (positive slope) curve observed, lying above the two-component prediction. Thus, we conclude that experimentally, we find an increased absorption coefficient in the dynamical hydration shell, α_{shell}, for all carbohydrates.

This is in disagreement with the results of our molecular modeling which yields an absorption coefficient, α_{shell}, that is apparently smaller than the bulk-water value. This may well be attributed to neglecting polarization effects in the force-field models, which influence the far-IR absorption band of water and water solutions, because polarizability has an impact on picosecond dynamics.[27] An example is the suppression of an absorption band around 150 cm^{-1} that is assigned to collective stretching modes of the hydrogen-bond network also involving intermolecular charge fluctuations.[28] The water potentials tested were SPC, TIP3P, and TIP5P, all of which were rigid and nonpolarizable. None accurately reproduced the far-IR spectrum, and no significant differences in our computational results were found for these force fields. It would be useful to carry out further studies by using polarizable force fields for the water or the carbohydrate and *ab initio* studies in the future.

The fitted width of the dynamical hydration shell for lactose is slightly larger than that observed previously, $\delta R = 5.7 \pm 0.4$ Å compared to $\delta R = 5.13 \pm 0.24$ Å. However, both results agree within their experimental uncertainties, which confirms our previous study. The final value for δR is correlated with the fitted value for $\Delta\alpha = (\alpha_{shell} - \alpha_{bulk})$, as can be seen in Figure 6. Because we measure the changes in the total THz absorption, a smaller value for $\Delta\alpha$ will yield a larger layer and vice versa. The more precise the measurements of the onset of nonlinearity, that is, the bending point and the curvature of the concentration-dependent measured THz absorption curves, the less δR and $\Delta\alpha$ are correlated with each other. We already investigated this correlation in our previous paper and came to the conclusion that, although a solvation layer of less than 4 Å is unlikely within the possible ranges for $\Delta\alpha$, a larger hydration shell of nearly 7 Å is still quite probable. As can be seen in Figure 6, the possible range is the largest for trehalose (extending between 5 and 8 Å) and the smallest for glucose (3−4 Å).

When we compare the results for the different carbohydrates, we find that trehalose and lactose, both being disaccharides, look very similar. Both have a similar long-range influence on the surrounding water, which extends beyond the first hydration layer. The THz absorption coefficient of water in the hydration shell increases within $\delta R = 5-7$ Å. The extension of this dynamical hydration shell is smaller for glucose than for the other carbohydrates. Monosaccharides have a smaller surface and fewer O−H bonds that can interact with the surrounding water. In the following, we search for a more-general correlation between the structure of the solute and the fast solvation dynamics.

Glucose has a volume that is a factor of 1.85 smaller than that of the disaccharides. This scaling factor is nearly the same

(27) Harder, E.; Eaves, J. D.; Tokmakoff, A.; Berne, B. J. *Proc. Natl. Acad. Sci. U.S.A.* **2005**, *102*, 11611–11616.
(28) Sharma, M.; Resta, R.; Car, R. *Phys. Rev. Lett.* **2005**, *95*, 187401.

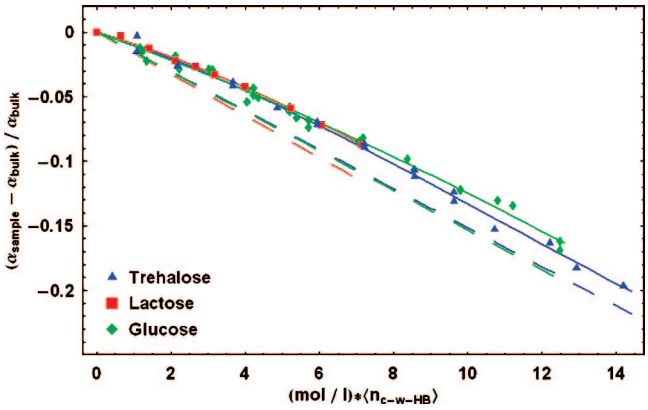

Figure 7. Difference in the integrated THz absorption coefficient (2.1−2.8 THz) relative to bulk water plotted against concentration. The molar concentration was multiplied by the average number of carbohydrate−water hydrogen bonds $\langle n_{c-wHB} \rangle$ for solvated trehalose (blue), lactose (red), and glucose (green). The experimental uncertainty for each measurement is smaller than the size of the dot ($\Delta((\alpha_{sample} - \alpha_{bulk})/\alpha_{bulk}) = \pm 0.008$). The temperature is kept at 20 °C. For comparison, the dashed lines show the prediction for a two-component model.

as the ratio of the available interaction sites suitable for forming hydrogen bond (as well as the mass ratio). The solute-induced changes should be directly correlated with the number of carbohydrate−water hydrogen bonds that can influence the water. In Figure 7, we have used the average number of carbohydrate−water bonds to scale our measured values. Instead of plotting the changes in the absorption against the molar concentration, we have plotted the changes in the integrated absorption against the molar concentration multiplied by the average number of carbohydrate−water hydrogen bonds, which is (according to our geometrical criterion as specified in the discussion) 7.02 for glucose, 11.62 for lactose, and 11.96 for trehalose and find a nearly perfect agreement for all three. These results show that the average number of carbohydrate−water bonds is the physical quantity that determines the long-range influence on the solvation dynamics for carbohydrates.

Computation of hydrogen-bond lifetimes between water molecules indicates retardation in hydrogen-bond breaking dynamics close to the solute. Fitting the hydrogen-bond correlation function obtained from MD simulations to $\exp(-t/\tau)$, we obtain $\tau = 1.5$ ps for bulk water, whereas we find values for the first solvation layer of 1.9, 2.1, and 2.1 ps for glucose, lactose, and trehalose, respectively. The results of the molecular modeling indicate significant retardation up to about δR from the solute.

In a modeling study of water near glucose, sucrose, and trehalose by Lee et al.,[9] a significant decrease in the translational diffusion coefficient for water molecules within about 5.5 Å from the surface of the solute was found. They computed the hydrogen-bond correlation function for the bonds between the hydration water and glucose and found retardation of the hydrogen-bond breaking dynamics between the solute and proximal water molecules, consistent with the results of our study. At 30 °C, the two disaccharides trehalose and sucrose studied in their paper were shown to retard the translational and rotational motions of the surrounding water molecules to a greater extent than glucose. The retardation of the hydration water in its rotational and translational motions is caused by the formation of carbohydrate−water bonds that are more stable than water−water bonds. The authors state that the glucose molecule forms comparably less-stable hydrogen bonds with the nearby water, which results in a less-pronounced decline in the water motions than those near disaccharides.

It is interesting to note that the increase in the range of influence on the solvation dynamics as found in this study correlates with increasingly effective bioprotection. This clearly supports the theory that the underlying molecular mechanism for bioprotection by addition of carbohydrates is the retardation of the solvent dynamics by sugars.

Summary

Our results show that disaccharides influence the fast (subpicosecond) hydration dynamics in their surroundings. We have determined the dynamical hydration shell for glucose, lactose, and trehalose. For disaccharides, we find that the THz absorption of the hydration water is increased in a range of 6−7 Å from the surface of the carbohydrate, which corresponds to about two hydration shells. For the monosaccharide glucose, we deduce a smaller extension of 3−4 Å. When comparing the concentration-dependent changes in the THz absorption for all three investigated solvated carbohydrates, we find that the total THz absorption for the mixtures can be correlated with the product of the molar concentration and the number of all hydrogen bonds formed between the solute molecule and water. We have compared this experimental result with the results of accompanying molecular modeling studies, which help understand the underlying physical picture.

Acknowledgment. We wish to thank Simon Ebbinghaus and Gerhard Schwaab for help in the instrument setup, analysis of the data, and software development. We thank Dominik Marx for helpful discussions. The authors also thank the Center for Bioinformatics at the University of Nevada, Reno, where some of the computational work was carried out. M. Heyden is thankful for financial funding provided by the DAAD and the Ruhr University Research School. M. Havenith and D. M. Leitner acknowledge financial support from the Human Frontier Science Programme.

JA0781083